UNIVERSITY of CALIFORNIA
SANTA CRUZ

# MODELING OF A PULSED HIGH MAGNETIC FIELD SOLENOID FOR ION BEAM FINAL FOCUS

A thesis submitted in partial satisfaction of the
requirements for the degree of

BACHELOR OF SCIENCE

in

PHYSICS

by

**Heaven L. Hodges**

4 October 2010

The thesis of Heaven L. Hodges is approved by:

| | |
|---|---|
| Frank Bieniosek<br>Advisor | Professor David P. Belanger<br>Theses Coordinator |

Professor David P. Belanger
Chair, Department of Physics

**Abstract**

Modeling of A Pulsed High Magnetic Field Solenoid for Ion Beam Final Focus

by

Heaven L. Hodges

The operational details of a proposed pulsed high magnetic field (50 T peak field strength) solenoid with flux excluder are explored. This device will be used for final focusing of the $Li^+$ particle beam that will be delivered by the upcoming NDCX-II induction accelerator at Lawrence Berkeley National Laboratory. Using the Poisson/Superfish Group Codes, peak field strength along the longitudinal axis, focal length, and pulse length were explored for a range of flux excluder geometries. Geometry variables included thickness (ranging from 0.5 mm to 4.5 mm) and the length of the excluders inner surface (ranging from 0.5 mm to 10 mm), while the outer radius and outer length were held constant at 5 mm and 10 mm, respectively. Results show that a thick flux excluder with a nearly triangular side perspective maximizes on-axis field strength and minimizes focal length ($\approx 0.108$ m); optimal measurements consisted of a thickness of 4.5 mm and an inner surface length of 0.5 mm. Scaling of all experimental field strength values such that this excluder has a peak on-axis field strength of 50 T suggests that $\approx 79,452$ A peak current must be achieved to drive the field. Field penetration of less than a tenth of the excluder's thickness necessitates a pulse length that is significantly less than 0.58 $\mu s$ if the concentrator is made of stainless steel and significantly less than 2.8 $\mu s$ for a tungsten excluder.

# Contents

**List of Figures** vi

**Dedication** vii

**Acknowledgements** viii

**1 Introduction** 1

**2 Method** 6

**3 Results** 12

**4 Conclusion** 18

**A Sample Automesh Input File** 20

**Bibliography** 22

# List of Figures

1.1 Flux Excluder: Head-On Perspective . . . . . 5
1.2 Flux Excluder: Half Longitudinal Slice . . . . . 5

2.1 Primary In Poisson Graphical Output with z = 30 mm by r = 45 mm Outer Geometry . . . . . 7
2.2 Primary with Pulsed Magnetic Field . . . . . 9
2.3 Primary with Steady-State Magnetic Field . . . . . 10

3.1 Comparison of On-Axis Magnetic Field Strength Distributions of Primary, Least Efficient Excluder, and Most Efficient Excluder . . . . . 13
3.2 Peak Field Strength On-Axis vs. L . . . . . 14
3.3 Peak Field Strength On-Axis vs. d (1 mm $\leq L \leq$ 5 mm) . . . . . 15
3.4 Peak Field Strength On-Axis vs. d (5 mm $\leq L \leq$ 10 mm) . . . . . 16
3.5 Focal Length . . . . . 17

4.1 Optimal Flux Excluder Geometry in Poisson Graphical Output . . . 19

Dedicated to Pascale Courtens

who,

in exhibiting interest in this project

despite a profound lack of understanding,

exemplified the nature of a true scientist.

# Acknowledgements

This research was accomplished at the Accelerator and Fusion Research Division of Lawrence Berkeley National Laboratory in Berkeley, CA between June 7 and August 13 of 2010 as a Science Undergraduate Laboratory Internship (SULI) project. The project was mentored by staff scientist Frank Bieniosek, with additional advising and inspiration provided by Enrique Henestroza. I thank the U.S. Department of Energy, the Center for Science and Engineering Education (CSEE) and LBNL for establishing, funding, and organizing the program.

# 1

# Introduction

As part of the Virtual National Laboratory for Heavy-Ion Fusion Science (HIFS-VNL) collaboration, the HIFS research group at Lawrence Berkeley National Laboratory (LBNL) is charged with contributing to the realization of controlled nuclear fusion for the ultimate goal of relatively inexpensive, readily available, non-toxic energy production. The group uses heavy-ion inertial confinement to drive the fusion of the plentiful hydrogen isotopes deuterium and tritium. In a single reaction of this kind, a small, frozen pellet of the deuterium and tritium "fuel" is housed in a Holraum metal shell and rapidly heated by intense ion beams from the Neutralized Drift Compression eXperiment (NDCX) induction particle accelerator. X-rays emitted by the heated Holraum shell compress the fuel pellet to such an extent that the fuel nuclei within fuse and release relatively large amounts of energy.

The achievement of this nuclear reaction is predicated upon the ion beam intensity. The positively charged lithium ions form a space-charge dominated beam that is

subject to spatial spread due to the electrically repulsive forces between the particles. Random thermal motion and thermal energy imparted by the ion source also affect beam spread. As ion beams from the NDCX lack the intensity to drive inertial fusion reactions, a new pulsed high magnetic field solenoid is being planned in anticipation of the projected 2012 arrival of the NDCX-II. NDCX and NDCX-II primarily utilize a negatively-charged plasma region to neutralize space charge repulsion. Fine radial focusing of the beam is subsequently accomplished with a pulsed, high magnetic field solenoid through which the beam passes near the end of its progress through the accelerator tube.

As the ion beam enters the solenoid (with a primarily longitudinally-directed velocity), the radial component of the cylindrically symmetric magnetic field imparts an azimuthal acceleration to the ion beam charge q according to the Lorentz Force Law (in cylindrical coordinates):

$$\vec{F}_\phi = q(v_z\hat{z} \times B_r\hat{r}) \tag{1.1}$$

Further along in the solenoid, where the longitudinal component dominates, the spiraling particles experience a radial force:

$$\vec{F}_r = q(v_\phi\hat{\phi} \times B_z\hat{z}) \tag{1.2}$$

and the resulting inward acceleration of the ions achieves radial compression of the beam, increasing the power per unit area delivered to the target.

It is estimated that the new final focus solenoid (FFS) should provide a 50 Tesla peak field strength along its longitudinal axis, a more than six-fold increase in relation to the field strength (8 T) of the solenoid currently in use. The design and construction of this component is complicated by the fact that such a high magnetic field strength will tend to destroy the solenoid that produces it, the Lorentz Force accelerating the solenoid's electrons in multiple directions at once. Resistance to this destructive force is a crucial factor in the design process, and materials such as stainless steel and tungsten have been proposed. The magnetic field is pulsed on a very short timescale, which prevents over-heating by the high current values necessary to produce such a large field, as well as the energy expense a constant field would necessitate. Furthermore, the magnetic field is timed to reach it's maximum strength when the ions pass through it; the periodicity of this traversal obviates the need for a constant field.

Modeling of the new solenoid was accomplished with the Poisson/Superfish group codes, which were developed at the Los Alamos National Laboratory. Taking inputs of solenoid geometry, materials, and current, Poisson calculates the strength of the magnetostatic field in user-specified regions within and near one or more field-producing device(s). This is accomplished by numerically solving Maxwell's equations via the method of successive over-relaxation. Only two-dimensional modeling is possible with the software.

The flux concentrator (or flux excluder) serves the purpose of focusing the magnetic field onto the longitudinal co-axis of the solenoid and excluder (the ion beam

path). It is therefore expected to increase the on-axis field strength, magnifying the effect that the solenoid alone would produce. The excluder will be air-insulated from the surrounding current-carrying coil. Viewed head-on (Fig. 1.1), the component resembles a hollow cylinder, but is unique in the design of its inner walls, whose length along the longitudinal axis varies with radial distance from the longitudinal axis. Visualizing the longitudinal slice in Fig. 1.2 revolved 360 degrees about the axis along which the inner length L lies clarifies this shape. The excluder also features a 1 micron wide cut that will force a return current to flow over the its inner surface in a direction opposite to that induced to flow over its outer surface. Estimations suggested a 10 mm outer length for the device. The outer radius was set at 5 mm. Variables explored in this investigation include the distance required to focus the ion beam (focal length) as a function of the driving current (via the induced magnetic field), and an upper limit on the appropriate pulse length of the driving current given two proposed construction materials, stainless steel and tungsten.

Figure 1.1: Flux Excluder: Head-On Perspective

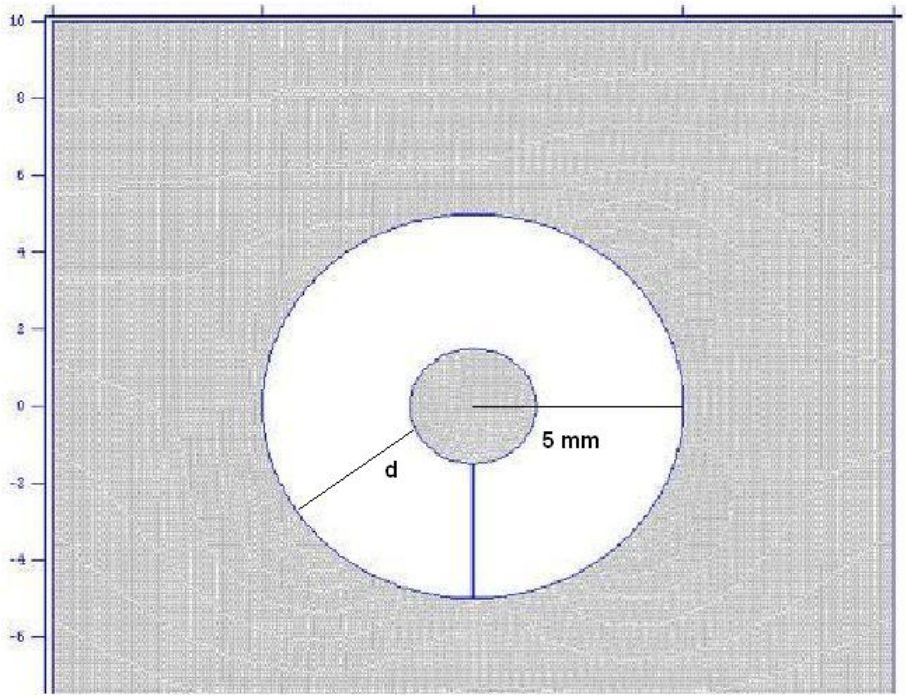


Figure 1.2: Flux Excluder: Half Longitudinal Slice

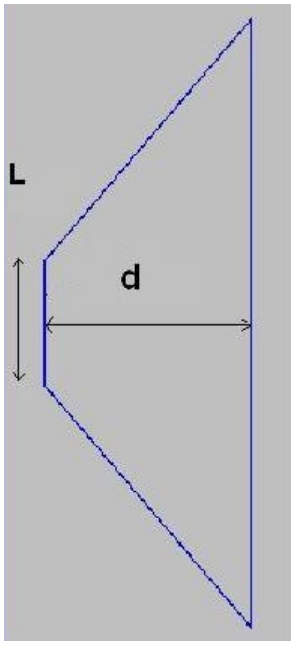

# 2

# Method

Due to the limited directions for current flow specification available in Poisson, the primary and flux concentrator were modeled from a side perspective only. A condition of cylindrical symmetry about the (vertical) z-axis was specified to simulate the three-dimensional nature of the physical problem, and thus only one half of the side perspective of the geometry appears in the output images.

The primary was modeled as a thin, rectangular tube (Fig. 2.1), 0.1 mm thick by 10 mm long, located a radial distance of 0.1 mm from the excluder. Revolved about the z axis, this model would form a single-turn coil, and was therefore expected to provide a field strength distribution closely approximating such a coil. The accuracy of Poisson's magnetic field strength calculations for the primary alone was verified by comparison with values predicted by [3]:

$$B(\zeta) = \mu_0 \frac{NI}{2\beta a} \frac{\Gamma(\alpha, \beta + \zeta) + \Gamma(\alpha, \beta + \zeta)}{2} \tag{2.1}$$

Figure 2.1: Primary In Poisson Graphical Output with z = 30 mm by r = 45 mm Outer Geometry

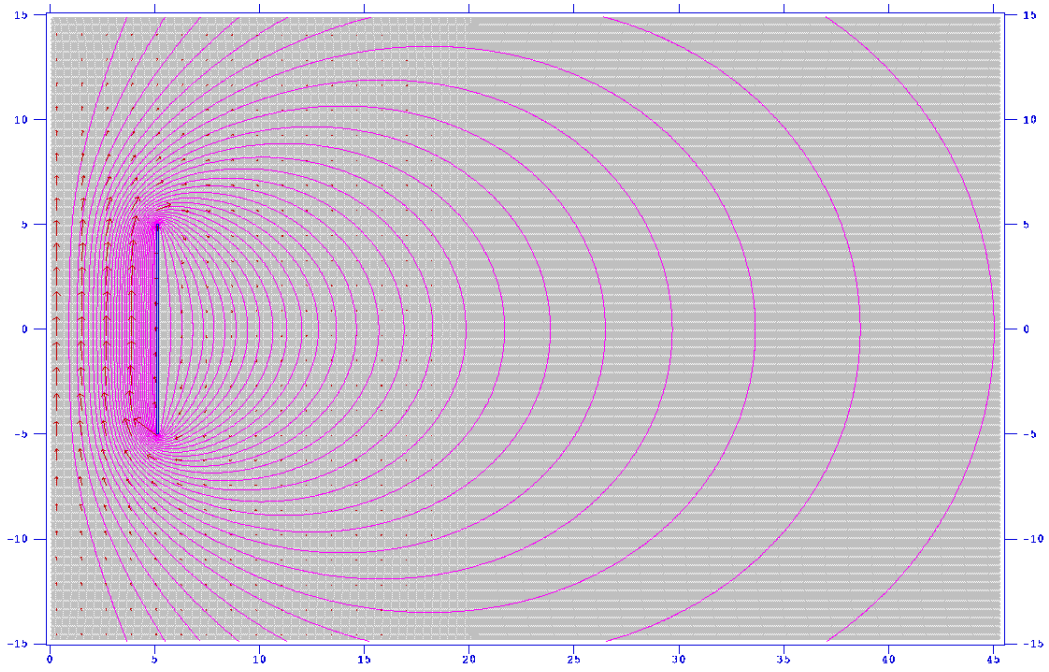


where $N$ is the number of turns (1), $I$ is the current input(1 A), $a$ is the inner radius of the coil (5.1 mm), $2\beta\alpha$ is its length (10 mm), $\alpha a$ is its outer radius (5.2 mm), $z = a\zeta$ is the distance from z=0, and

$$\Gamma = \frac{\beta}{\alpha - 1} ln \frac{\alpha + \sqrt{\alpha^2 + \beta^2}}{1 + \sqrt{1 + \beta^2}} \tag{2.2}$$

As Poisson is only capable of steady-state simulations, only the peak of the pulsed field was modeled. A magnetic field that is pulsed with sufficient rapidity will penetrate the excluder very little, and the field within the flux excluder boundary would be zero. The condition of minimal penetration was simulated by setting the excluder boundary to a fixed vector potential (input parameter IBOUND=-1, see Appendix A). The value specified for this potential (input parameter CUR) was also interpreted by Poisson as the magnitude of the total current on the flux excluder surface.

Poisson altered the field due to this surface current to create the constant surface potential; this in turn altered the field distribution (in relation to the field that would have existed without the IBOUND specification). It was therefore necessary to scale the on-axis field strength magnitude (there was little concern with the off-axis field aside from its realism) at each of the chosen sample points $z$ such that, according to Ampere's Law

$$\frac{\int_{\infty}^{\infty} B_z dz}{\mu_0}$$

was constant across all Poisson trials, as it was desired to run all trials with the same peak driving current.

It is expected that the on-axis value of $\int B_z dz$ for the flux excluder approach the value of the same for the primary alone in the limit $d \to 0$. After the aforementioned scaling in accordance with Ampere's Law, there was a discrepancy of a factor of approximately 11 between the values of this integral for the coil and for the trial excluders for which d=0.5 mm (interpreted as an approximation to d=0). This necessitated the specification of a fixed potential over the surface of the primary as well, which ameliorated the discrepancy by increasing $\int B_z dz$ for the primary by a factor of about 9.56. The physical significance of this simulation detail (zero field penetration within the coil due to a pulsed field) not only increased the realism of the simulation, but is desirable from a design perspective. Figs.s 2.2 and 2.3 show the difference in field configuration of the coil with and without magnetic flux excluded. All magnetic field strength values were then scaled such that the peak on-axis field strength of the best field-concentrating excluder was equal to 50 T. Ampere's Law

Figure 2.2: Primary with Pulsed Magnetic Field

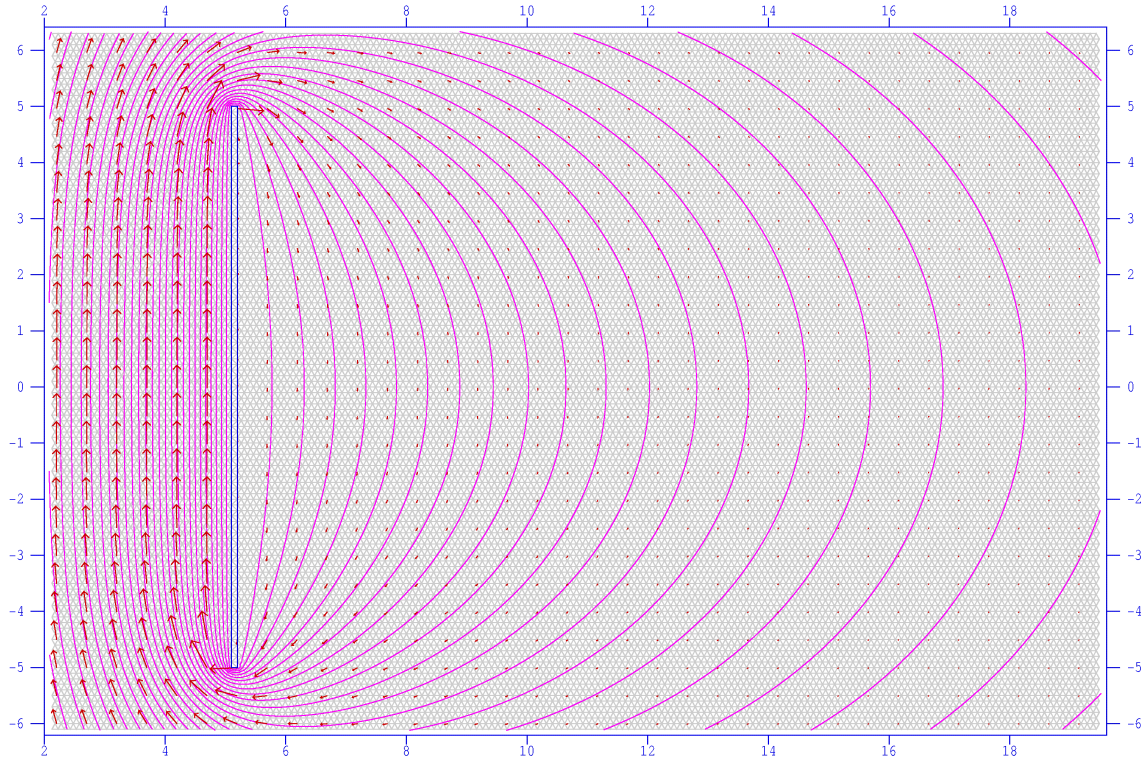


revealed that this resulted in an effective input current of $\approx 7.96 \times 10^4$ A.

If the current is pulsed on a sufficiently short time scale, the strength of the magnetic field will be sufficiently attenuated to allow one to avoid significant field penetration. It is therefore required that the penetration depth $\delta$ [2] of the field remain significantly less than the thickness d of the flux concentrator:

$$\delta = \frac{k}{\sqrt{f}} << d \tag{2.3}$$

for the material-dependent constant k. The frequency f of the current pulse is related to the duration of the pulse $\tau$ by

$$f = \frac{1}{2\tau} \tag{2.4}$$

Figure 2.3: Primary with Steady-State Magnetic Field

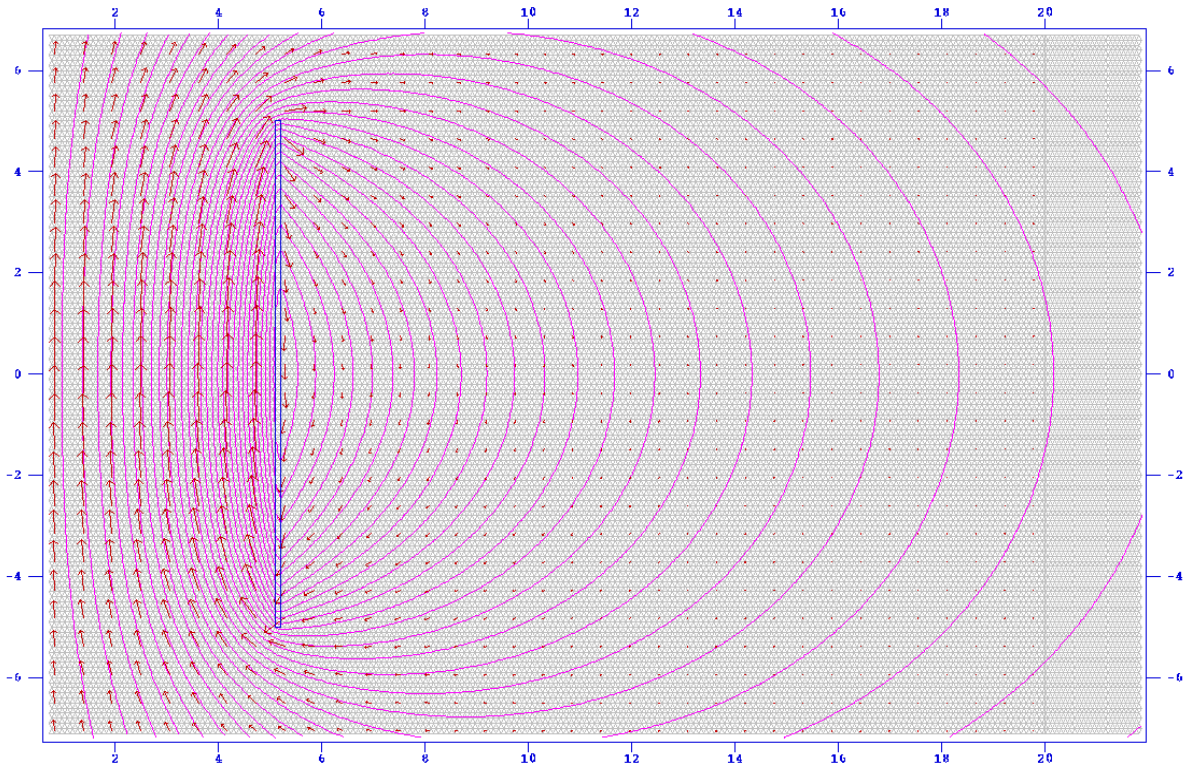


Equations 2.3 and 2.4 lead to the relationship:

$$\tau << \frac{d^2}{2k^2} \tag{2.5}$$

For stainless steel, $k = 0.417$; for tungsten, $k = 0.189$.

Flux excluder geometry was varied to determine it's effect on magnetic field strength. While holding the outer radius constant at 5 mm, the radial thickness of the excluder, d, ranged from 0.5 mm to 4.5 mm in 0.5 mm increments. The length of the shorter base in the trapezoidal side perspective, L, varied from 0.5 mm to 10 mm in 0.5 mm increments (Figure 1.2). The combination of these two variables produced a total of 180 physically distinct possible flux excluders. The Poisson/Superfish

post-processor SF7 supplied the values of $B_z$ at 1000 evenly-spaced intervals along the longitudinal axis ($-100$ mm $< z <$ 100 mm) in each of these trials. These values were then used to calculate the focal length [1],

$$f = \frac{4}{\int \left[\frac{qB_z(0,z)}{\gamma m_0 v_z}\right]^2 dz} \tag{2.6}$$

where $m_0$ is the relativistic mass of the ions ($Li^+$), $v_z$ is their longitudinal velocity, and $\gamma$ is the Lorentz factor. The latter two constants were calculated using the ion kinetic energy of 2 MeV . The charge q of one ion is 2e.

# 3

# Results

While agreement between experimental and theoretical field strength values for the primary was very good for on-axis points near the origin, over 50% of the points at which the field strength was sampled disagreed with Equation 2.1 with greater than 20% error, regardless of the number of points sampled. Due to the feature of Poisson that forces the magnetic field strength to approach zero near the limits of the outer geometry, this was especially true near $z = \pm 100$ mm, where relative error exceeded several hundred percent, in comparison with about 2.5% relative error at $z = 0$. Equationtheory does not apply to a pulsed primary, and so there was no agreement after scaling of the field strength values via Ampere's Law.

Figure 3.1 illustrates the expected increase in magnetic field strength afforded by the inclusion of a flux excluder in the solenoid construction. The factor of increase of peak on-axis ($B_{z=0}$) field strength ranged from $\approx 1.03$ (for L=10, d=0.5) to $\approx 8.02$ (L=0.5, d=4.5).

Figure 3.1: Comparison of On-Axis Magnetic Field Strength Distributions of Primary, Least Efficient Excluder, and Most Efficient Excluder

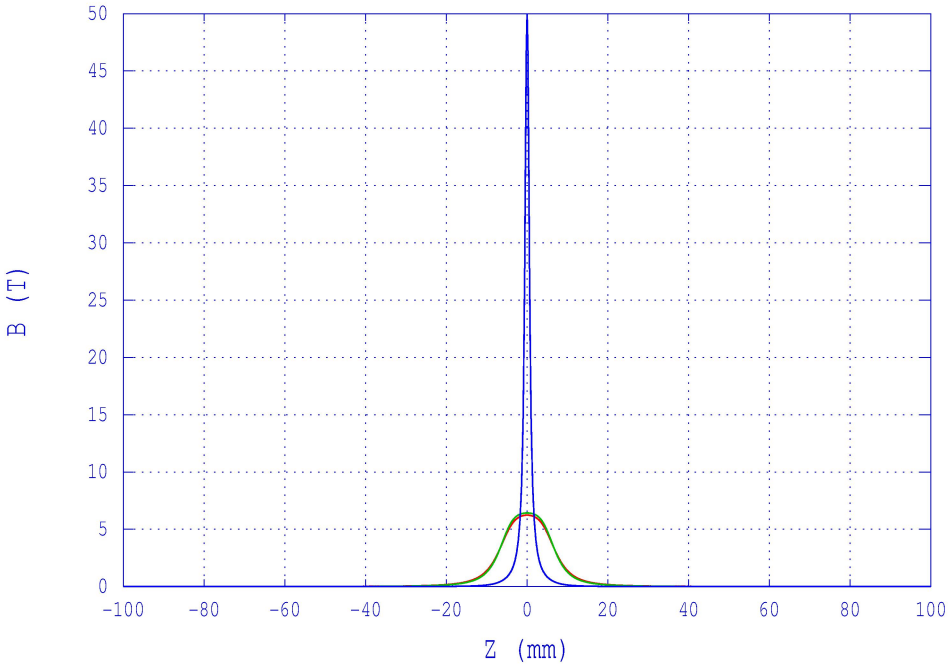

Figure 3.2: Peak Field Strength On-Axis vs. L

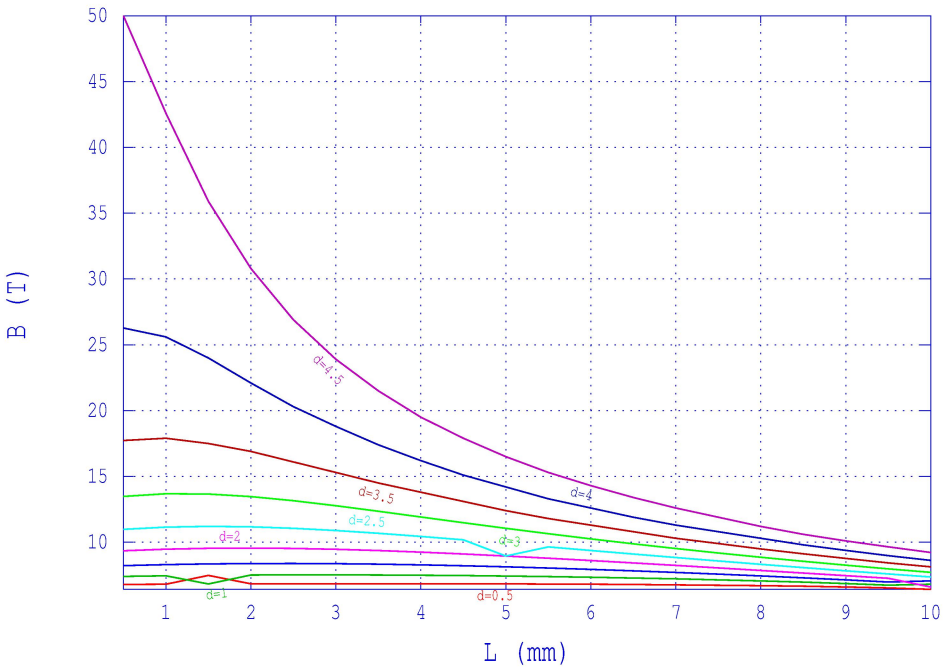


The relationship between peak on-axis field strengths for the 180 different geometries can be seen in Figs.s 3.2, 3.3 and 3.4.

The peak field as a function of d for L=0.5 mm through L=5 mm is presented in Fig. 3.3. Figure 3.4 shows the same relationship for L=5.5 mm through L=10 mm.

Figure 3.5 shows the variation of focal length as a function of L.

Figure 3.3: Peak Field Strength On-Axis vs. d (1 mm $\leq L \leq$ 5 mm)

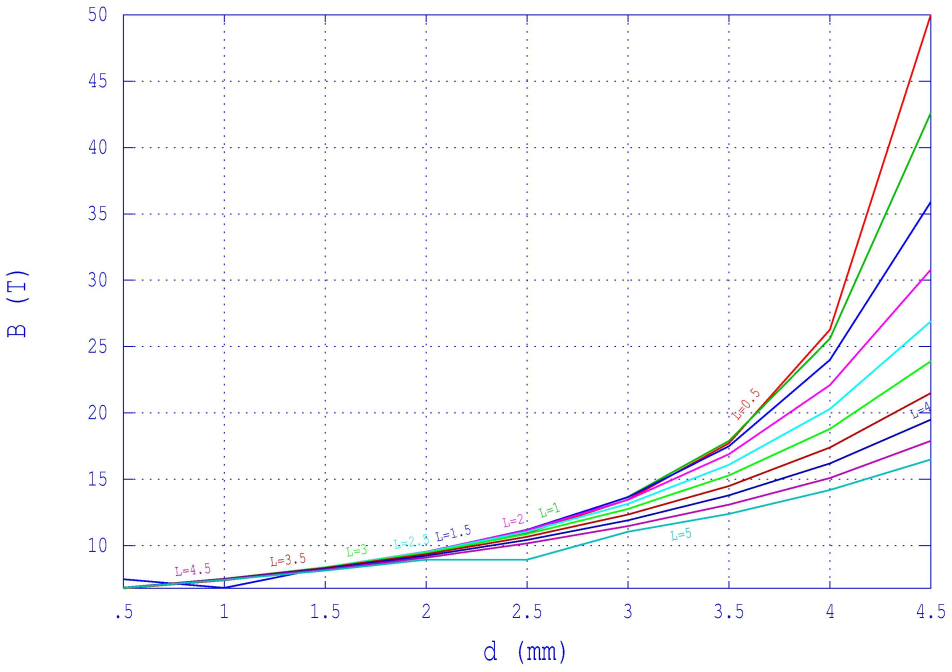

Figure 3.4: Peak Field Strength On-Axis vs. d (5 mm $\leq L \leq$ 10 mm)

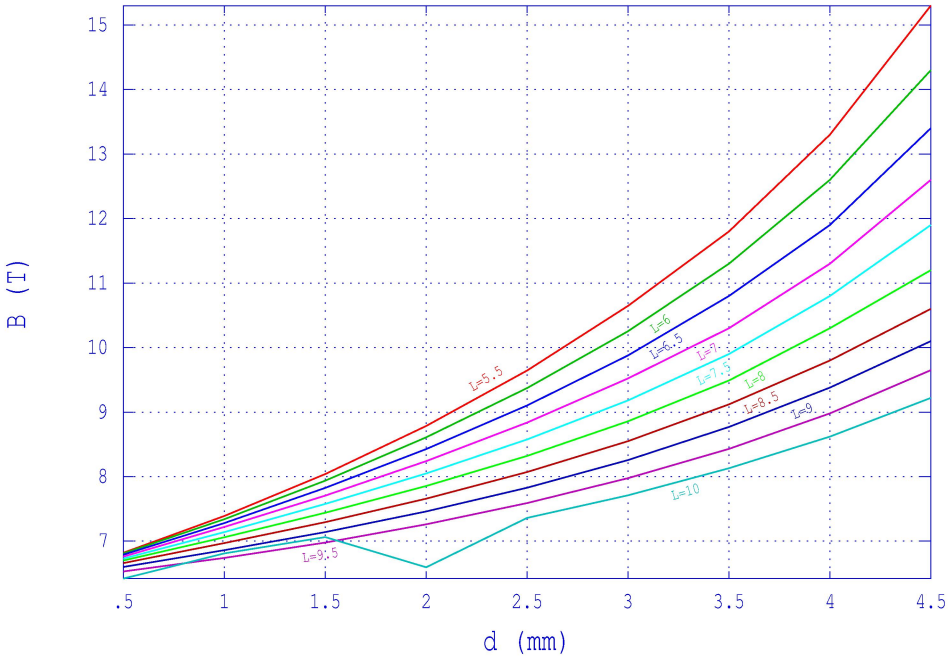

Figure 3.5: Focal Length

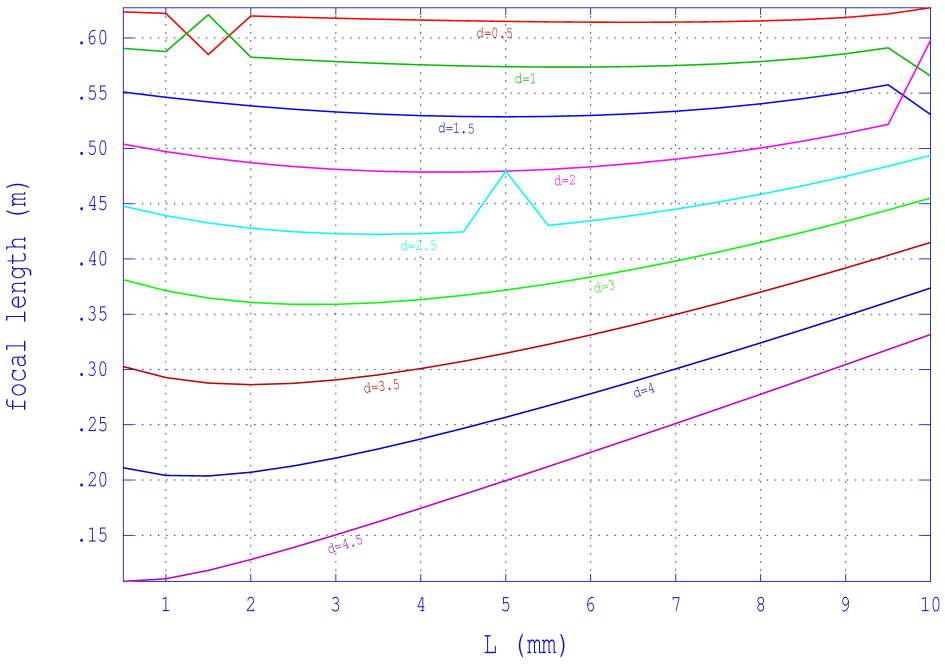

# 4

# Conclusion

The substantial disagreement between experimental and theoretical (Equation 2.1) field strength calculations suggests an increase in the size of the outer geometry (with respect to the solenoid and flux excluder) and the number of sample points along the longitudinal axis as much as possible in any future investigations of a DC-driven primary.

As it is clear from Fig. 3.1 that the inclusion of a flux concentrator will increase the efficiency of the proposed FFS, it remains to decide on the details of the construction of the device. The dependence of the peak field strength on the parameter d suggests that the thickest flux concentrator that is practical would maximize the field on-axis. Further investigation should take into account the minimum radius of the aperture necessary for beam traversal, as the possibility of beam interaction with the current-carrying walls of this aperture is undesirable.

According to Equation 2.5, taking d=4.5 mm as the appropriate thickness of the

Figure 4.1: Optimal Flux Excluder Geometry in Poisson Graphical Output

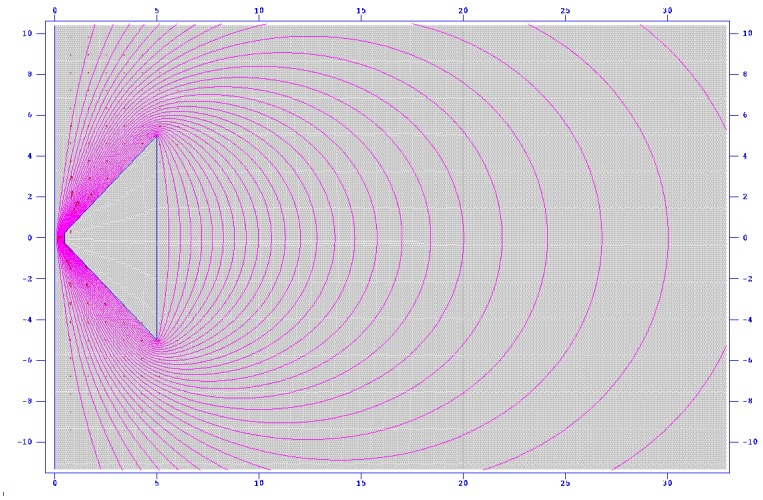

excluder constrains the pulse length by

$$\tau << \frac{(0.45 \text{ mm})^2}{2(0.417)^2} \approx 5.82 \times 10^{-7} \text{ s}, \tag{4.1}$$

for steel and

$$\tau << \frac{(0.45 \text{ mm})^2}{2(0.189)^2} \approx 2.834 \times 10^{-6} \text{ s}, \tag{4.2}$$

for tungsten, assuming the upper limit on the pulse length is at least 10 times smaller than d.

The graphs clearly show that the peak on-axis field strength would be a achieved with with $d = 4.5$ mm, $L = 0.5$ mm. The minimum focal length ($\approx 0.108$ m) also coincides with these measurements. If one were to slice this excluder in half and then in fourths along its longitudinal axis, one would see the figure presented in Fig. 4.1, which is presented with its magnetic field.

# Appendix A

# Sample Automesh Input File

```
Flux Concentrator with Surface Current (Side Perspective)

$REG KPROB=0,
ICYLIN=1,
DX=0.025,
DY=0.025,
NBSLF=0,
NBSLO=0,
YREG=-50.0, -15.0, 15.0, 50
LREG=0, 50, 210, 510, 670
LMAX = 720
XREG=20.0, 50
KREG=0, 200, 550
KMAX=600
CONV=0.1  &

&PO X=0.0, Y=-100.0 &
&PO X=100.0, Y=-100.0 &
&PO X=100.0, Y=100.0 &
&PO X=0.0, Y=100.0 &
&PO X=0.0, Y=-100.0 &

&REG CUR=1 IBOUND=-1 &
;flux concentrator

&PO X= 0.5 ,Y= -0.25 &
```

```
&PO X= 5 ,Y= -5 &
&PO X= 5 ,Y= 5 &
&PO X= 0.5 ,Y= 0.25 &
&PO X= 0.5 ,Y= -0.25 &
```

# Bibliography

[1] S. Humphries, Jr. *Principles of Charged Particle Acceleration*. New York: John Wiley & Sons, 1986, pp. 127.

[2] S. Ramo, J. Whinnery, and T. Van Duzer, *Fields and Waves In Communication Electronics*. New York: John Wiley & Sons, Inc., 1965, pp. 289.

[3] F. Herlach *Pulsed Magnets*. New York: John Wiley & Sons, Inc., 1965, pp. 864.